

Design of an MRI Compatible Haptic Interface

Melih Turkseven and Jun Ueda

Abstract— This paper proposes an MRI-compatible, 1-axis force sensing unit which is designed to be used as a haptic interface on an MRI compatible robot. Recently, it became a popular research direction to enable MRI in surgical operations and brain studies with the help of robotic devices. However, due to high magnetic field in MRI environment, conventional sensors and robots cannot be used in MRI rooms. Existing MRI-compatible force sensors have limited number of degrees of freedom or they do not offer compact solutions for multiple-axis sensing. In this paper, a compact 1-axis force sensing unit which employs a compliant displacement amplification mechanism is introduced and then analyzed for better sensitivity and accuracy. A combination of multiple proposed sensing units can be assembled to have a force sensor with desired number of degrees of freedom. Prototypes made of delrin and ABS-plastic are tested. Experiments indicated that the proposed sensor is suitable for force sensing and fully compatible to MRI. Also, the sensor made of delrin is superior in mechanical performance and MRI compatibility to ABS-plastic sample.

I. INTRODUCTION

Magnetic-Resonance Imaging (MRI) has become a widely applied tool for diagnostics as it provides real-time, high definition and highly accurate information about soft human tissues. However, due to high magnetic field and RF pulses inside MRI chamber, conventional robots with conductive and ferrous materials cannot function properly. Recently, it has been a new challenge for researchers to develop MRI-compatible robotic devices in order to extend MRI's role to brain studies and surgeries. There are various robotic devices designed for certain surgical operations inside an MRI chamber. Gassert *et al.* developed a robotic system for general MRI studies [1], Ho Tse *et al.* designed an MRI compatible robot to adjust position of patient's limb for highest accuracy in images [2].

Force feedback is a crucial element for medical robots as it provides operators with sense of touch. Wagner *et al* [3] described the advantages of force feedback during blunt dissection. A sense of touch prevents the surgeon damage the soft, vulnerable tissue during dissection. In order to be effective and sensitive, the force sensor should be integrated

Manuscript received March 28, 2011. This work was supported in part by the National Science Foundation Engineering Center for Compact and Efficient Fluid Power (CCEFP).

Melih Turkseven and Jun Ueda are with George W. Woodruff School of Mechanical Engineering, Georgia Institute of Technology, Atlanta, GA, 30332-0405 U.S.A. (e-mail: mturkseven3@ gatech.edu & jun.ueda@me.gatech.edu).

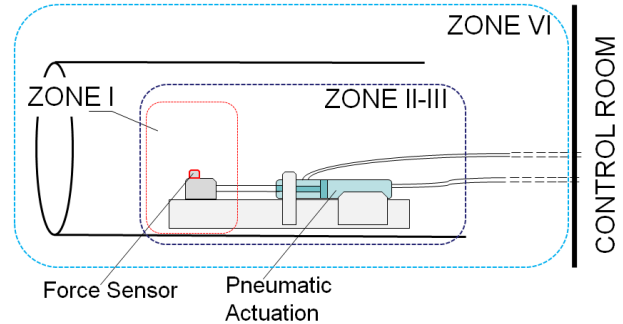


Fig. 1. A schematic for the MRI-compatible robot with force feedback. Definitions of the zones shown in this figure are given in 'MRI Safety' part.

to the end effector of the device. Since end effectors are usually in touch with the patient and extremely close to the area of interest, the sensor should be harmless to the patient and MRI machine. The proposed force sensor is planned to be used on a pneumatically actuated MRI-compatible robot to enable force feedback. Figure 1 illustrates the relative location of a force sensor attached on a robot inside MRI room. Such a robot with haptic interface to be used by the patient inside MRI chamber enables fMRI studies on somatosensory system or could be used as a platform for surgeries. The geometry of compact body of the sensor can be modified to confirm restrictions on various applications. Since the volume inside MRI machines is quiet tight, such force sensors or haptic interfaces have to be small-sized.

Several models of MRI-compatible force sensors are catalogued by Gassert *et al.* [4]. Puangmali *et al* developed a 3-axis force sensor for minimally invasive surgeries [5]. Chapuis *et al.* developed a force/torque sensor [6], Khanicheh *et al.* designed a hand driven haptic interface which employs ERF fluids [7], Xuan Tan *et al.* introduced a triaxial force sensor using displacement amplification mechanisms [8]. However, these design ideas are not meant for extension to 6-axis sensing applications. Tada *et al.* introduced different models for 2-3 axis sensing [9,10] and developed a 6-axis force sensor [11] yet these designs impose many inputs to be handled and multiple cables for fewer number of axis force sensing. Also, significantly high hysteresis seems to be a common, inevitable problem for plastic MRI-compatible sensors.

This paper proposes a compact, 1-axis fiber optic force sensing unit that can be easily extended to multi-axis designs. Design of the 1-axis sensing unit and its suitability for extension to multi-axis sensing are primarily discussed. Since the volume inside MRI chamber is tight, a compact sensor body is aimed. The sensing principle of the proposed design is chosen to minimize the cable traffic and input handle. A genuine displacement amplification compliant mechanism is designed to increase the sensitivity in the axial

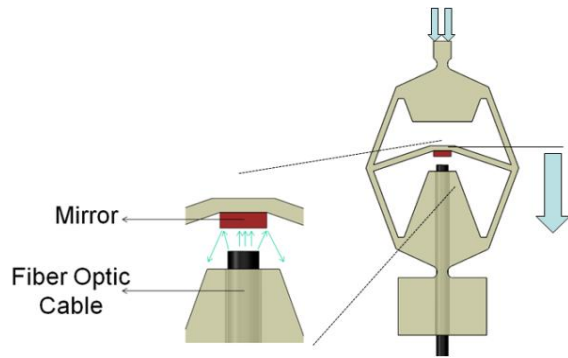


Fig. 2. Deformable structure of the proposed sensor

direction exclusively and reduce hysteresis. A displacement amplification mechanism would reduce the total strain energy deployed on the sensor body by increasing the sensitivity of the sensor, alleviating the hysteresis problem. In this work, that sensor body is analyzed for higher accuracy and amplification performance. MRI compatibility and mechanical performance of this sensing unit under axial and lateral loading are tested.

MRI Safety

The high magnetic field and RF pulses inside MRI room interfere with electrically driven sensors and robots. Either the robotic device is affected by the MRI machine or the device causes distortion in the output image of the MRI machine. Detailed explanations on the requirements for MRI-compatibility have been shown in various sources [12-14].

The material of the device should be magnetically inert. A non-compatible device itself can be attracted by the MRI machine which may induce a dangerous action called missile effect. Also a magnetic piece distorts the output images since magnetic field inside the MRI machine loses its homogeneity. Non-conductive materials are advantageous about compatibility. Magnetic field can induce Eddy current on the conductive body of the device. That may heat the device which may become dangerous especially if that device is in contact with patients.

The severity of the restrictions for MRI-compatibility depends on how close the device is to the area being imaged. In this paper, following definitions for different compatibility levels are accepted [14].

Zone 1 device: Operates in the area being imaged. Usually in contact with the patient, a device working in this region should be highly compatible to MRI environment.

Zone 2 device: Remains inside the MRI chamber but not in the area being imaged.

Zone 3 device: Remains inside the MRI chamber but not in use during imaging

Zone 4 device: Can be used inside MRI room as long as it is kept a distance of more than 1 m to the magnet bore. These zones are illustrated in Figure 1.

II. SENSING PRINCIPLES

The proposed sensing principle is shown in Figure 2. A mirror and a fiber optic cable are assembled on a deformable structure. As in almost every force sensors, an applied force deforms the structure moving the mirror with respect to the

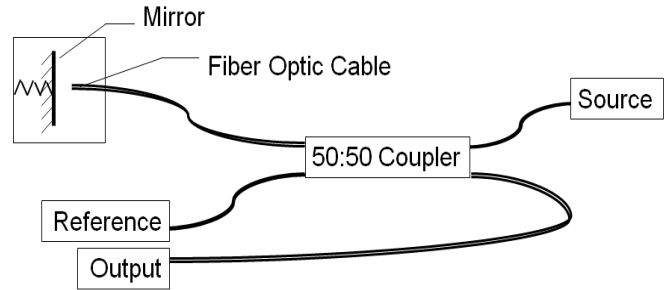


Fig. 3. Fiber Optic Circuitry for the proposed sensor. The intensity of the light at output port with respect to the reference port is measured.

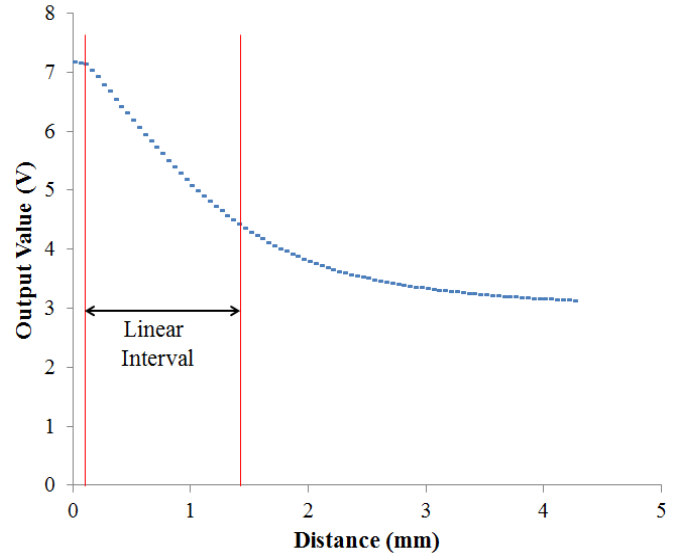


Fig. 4. Light intensity measurement. The output changes in a linear fashion between 0.1-1.5 mm of distance between fiber tip and mirror.

fiber optic cable. A genuine compliant mechanism is designed to amplify the displacement of the mirror in axial direction. As the gap between the fiber tip and mirror changes, the intensity of reflected light varies. The reflected light is transmitted via the same fiber optic cable through a fiber optic circuit. The circuit involves 2 photodiodes, a light source and a bi-directional fiber optic coupler. Figure 3 shows a simplified schema of the circuit which was examined by Lazeroms *et al.* [15]

Fiber to mirror assembly offers an easy and compact way to sense the deflection in the body. The variation in the output voltage and the distance between mirror-fiber couple is illustrated in Figure 4. To have a linear variation with high sensitivity 0.1-1.50 mm interval is chosen for the assembly.

III. STRUCTURE

A deformable structure is developed to transduce the force into displacement. To have a good resolution the displacement should be high and overall stiffness of the body should be low. Also, an ideal 1-axis sensor is only sensitive in one direction. Considering these facts, a new displacement amplification compliant mechanism (DACM) is designed for sensing purposes. In order to optimize the initial design idea, significant geometric parameters of the structure is derived by a trivial kinematic analysis. Then the

performance of the design is optimized by playing with those parameters using finite element analysis software. Due to elastic deformation in the body, kinematic models do not represent the structure but may reveal effective parameters. Figure 5 contains a 2D sketch of the mechanism as well as five most significant parameters on it.

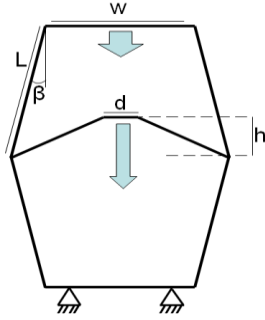


Fig. 5. 2D sketch of the mechanism. L , d , w , h represent size of relevant bars and β is the angle as shown.

Initial kinematic analysis yielded the following equation for the amplification ratio:

$$\text{Amplification} = \frac{L \sin \beta + \left(\frac{w-d}{2}\right) \cot \beta}{h} \quad (1)$$

Table I presents an optimal set of dimensions for chosen limits for the overall length and width of the body maximizing the resultant amplification ratio.

TABLE I
Nominal Values of Design Parameters

Symbol	Explanation	Value
L	Length of side bars	15 mm
w	Width of the top bar	15 mm
h	Distance between middle bar and Mid-line of the model	3 mm
β	Angle between side bar and top	20°
d	Length of middle bar	3 mm

Series of simulations showed that amplification ratio increases as length (L) and width (w) of the body are raised but other parameters do have certain optimum values. To define a limit to overall size of the sensor, length and width of the lateral links are limited to 15 mm manually. In order to avoid energy absorption by unwanted internal elastic deformations, the top and bottom part of the body is strengthened by adding more material.

Available fabrication methods for the designed structure become a matter to consider if the material of interest is plastic. Fabrication opportunities vary with the type of plastic and fabrication type is a significant factor on the performance of the sensor. Delrin (Acetal) has high MRI-compatibility and relatively low hysteresis characteristics yet delrin could be cut to precision only by water jet cutter. Water jet cutter has significant resolution limits compared to laser cutter or rapid prototyper. Whereas ABS-plastic is a cheap material and a complicated, 3D structure can be produced in rapid prototyper easily; but that does not guarantee better mechanical performances. Finite element simulations for two loading conditions have been made: axial loading and lateral loading cases. Figure 6 illustrates the

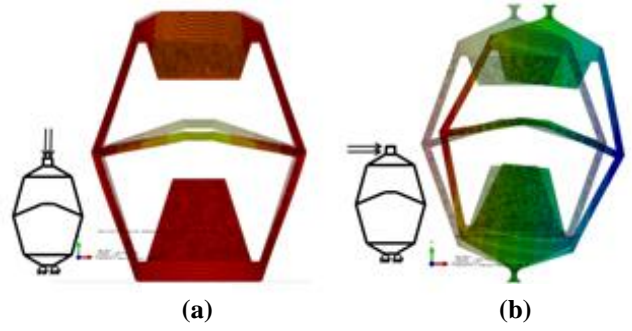


Fig. 6. Finite element models a) Deflected shape after axial loading b) deflected shape after lateral loading. Under a lateral load, orientation of fiber tip with respect to mirror does not change significantly

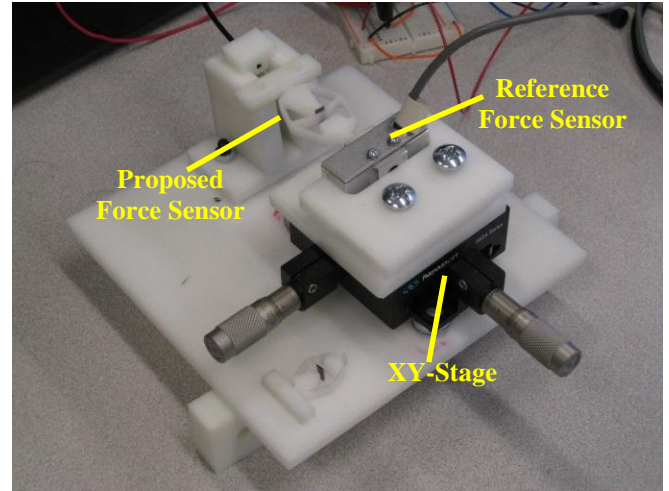


Fig. 7. Experimental apparatus for mechanical testing of sensing units. Known deformations are induced by an XY-stage aligned to the sensor and the calibration data is received by a commercial force sensor.

boundary conditions of the models and loading configurations for each type of simulation along with the images of deflected model.

IV. EXPERIMENTAL SETUP

A number of mechanical tests have been made to check the sensitivity of the structure in axial and lateral directions. The fiber optic cable is a plastic 900 μm fiber from Industrial Fiber Optics Co. and the fiber optic coupler is 50:50 IF-540 from the same vendor. The light source is 5 mW red lasers from Lasiris Inc. A magenta, silicon mirror is used in the experiments. The 1-axis sensing unit is fixed to a plastic frame as seen in Figure 7 since a real application would also be a fixture to a plastic frame. A load cell, OMEGA-DYNE LCM703-50, is attached to a linear XY-stage and positioned next to the sensor. The sensor is compressed via the linear stage in axial and lateral directions to realize the configurations in finite element analyses. The tests are done on two sensors with the same geometry but different materials. One acetal delrin piece and an ABS-plastic piece are tested under the same conditions. The output from the photodiode of the optic circuitry is amplified by an electronic circuit. The data is collected by National Instruments USB-6221 data acquisition device.

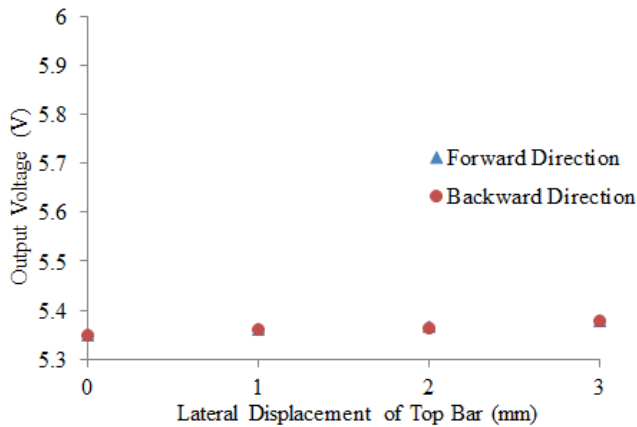
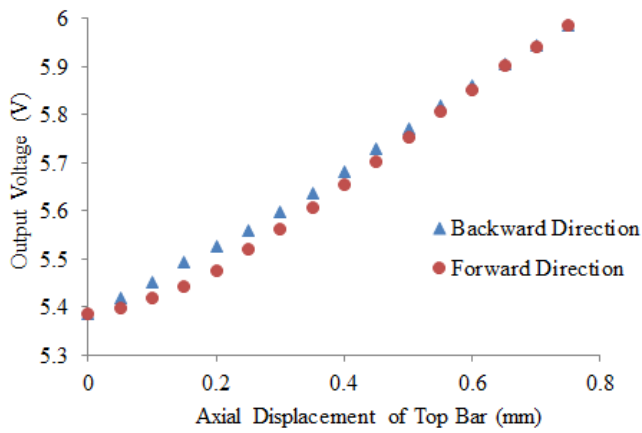


Fig. 8. Output voltage vs. displacement diagram that presents several loading-unloading cycles for delrin sample. The diagrams indicate that the sensor can decouple lateral load. a) Axial loading experiment. b) Lateral loading experiment. No hysteresis is seen in lateral loading case.

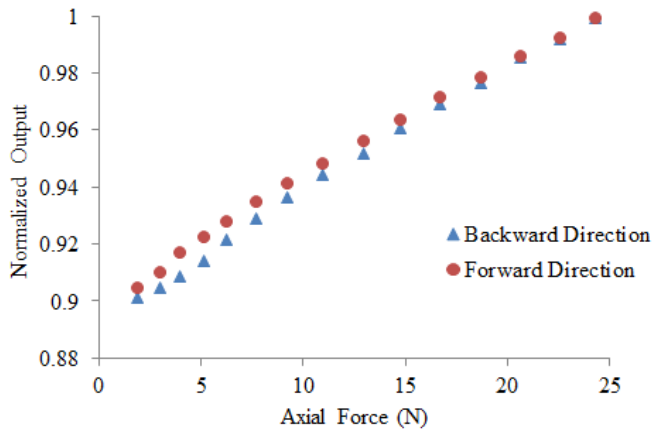


Fig. 9. Calibration data for the sensor made of delrin. Hysteresis is seen in 0-5 N range. The output voltage is linear with respect to the force.

V. CALIBRATION

Figure 8 illustrates the results of axial loading and lateral loading experiments conducted on delrin structure. Comparing the plots in Figure 8 the structure is concluded to be very well capable of decoupling axial and lateral forces. For 1 mm of displacement, the variation in lateral loading case is 1.66% of the variation in axial displacement. However, it is also evident that only a portion of the compression is absorbed by the sensing mechanism and the

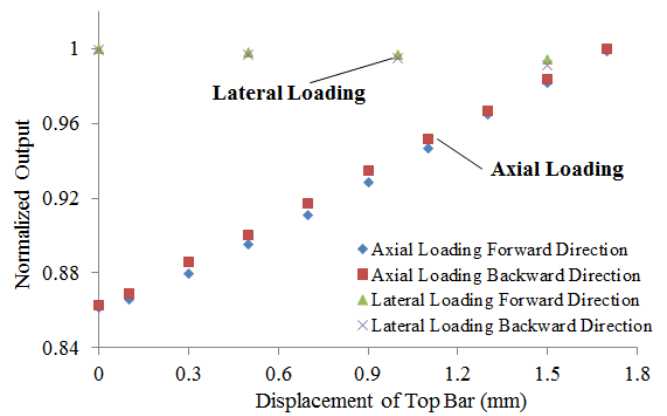


Fig. 10. Output voltage vs. displacement diagram for both axial and lateral loading tests for ABS-plastic sample. The diagram involves several loading-unloading cycles for each loading case.

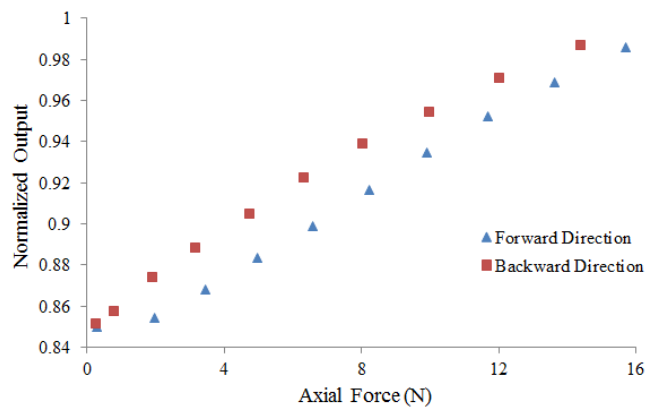


Fig. 11. Calibration data for the sensor made of ABS-plastic. Hysteresis is a more significant problem for ABS-plastic sample compared to the delrin sample

rest is absorbed by the fixture of experimental setup. The total displacement of the top of the sensor exceeds the length of the gap between fiber and the mirror which implies that the whole setup deflects during the experiment. The diagram in figure 9 presents the calibration data of the device made of delrin under axial loading. The output of the sensor is linearly related to the force. Yet, a certain amount of hysteresis, 4.99%, is evident.

The plots in Figure 10 and 11 show the output of same axial and lateral loading tests applied on the sensor made of ABS-plastic. Figure 10 presents both axial and lateral loading experiments revealing that the ABS-plastic sensor is also capable of decoupling axial and lateral forces. For 1.7 mm of displacement, the variation in lateral loading case is 3.29% of the variation in axial displacement. Figure 11 demonstrates the force sensing performance of the sensor. Stiffness of the ABS-plastic piece is lower yet the hysteresis is significantly higher compared to delrin piece. The hysteresis in ABS-plastic sample is 13%.

V. DISCUSSION

This 1-axis sensing unit is proven to be suitable for force sensing applications. Since the structure can decouple lateral loads, a combination of such structures can be used for multi-axis applications. Delrin presented better mechanical

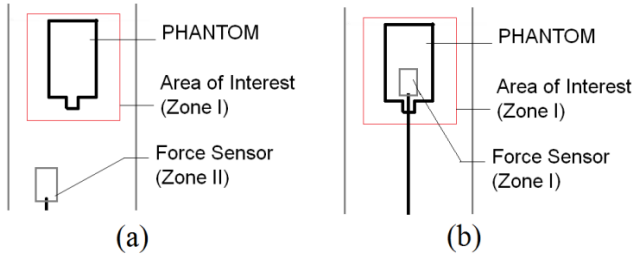


Fig. 12. Configuration inside MRI chamber **a)** Force sensor is placed in Zone II **b)** Force sensor is placed in Zone I, right on top of the phantom device

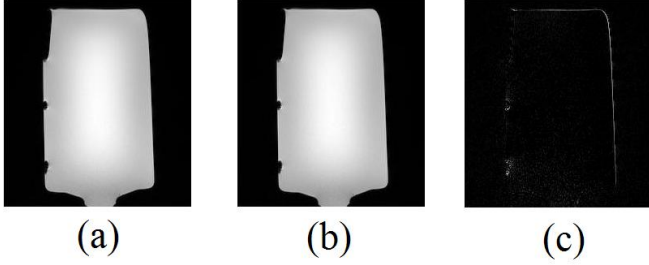


Fig. 13. **a)** MR image when sensor is not in the room **b)** Image when the sensor is in zone II **c)** The subtraction a-b, the difference is 0.5%

performance compared to ABS-plastic in both hysteresis and decoupling. Linearity in the output of the delrin piece is also satisfactory. On the other hand, the stiffness of the delrin structure is too high for a haptic application and should be lowered. It was observed that, whole experimental setup was deflecting during the axial loading experiment as the sensor was fixed to a plastic (delrin) frame. Although that might seem as a drawback, it is realistic since the plastic force sensor is going to be attached to another MRI-compatible frame which is likely to be plastic. The rigidity of the frame is another important fact to be improved for higher accuracy. Hysteresis and repeatability characteristics of the device should also be further improved.

VI. MRI COMPATIBILITY

In order to confirm the MRI-compatibility of the sensing unit, several imaging tests have been done. The sensing unit was brought to an MRI machine (Siemens Trio 3T) in the Center of Advanced Brain Imaging. Effect of the sensor on the image quality is analyzed by comparing the images of the PHANTOM device with and without the sensor in the imaging room. First, the sensor is placed in zone 2 and then the sensor is placed in the middle of the area of interest (Zone 1) as shown in Figure 12. This procedure was repeated for both delrin and ABS-plastic sensors.

Figure 13 and 14 present the resultant images of the tests for the two configurations shown in Figure 12. The distortion due to the force sensor is analyzed by taking the difference between related images. As a preliminary analysis, the differences in the images are calculated as the ratio of total pixel value of difference in images with respect to total pixel value of the reference image. The sensor, made of delrin, caused only 1.6% of change in the image even when it is held in the area of interest (Zone I). To present a more reliable indicator for the difference in the images, SNR

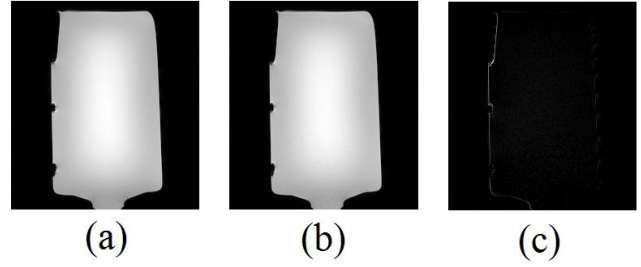


Fig. 14. **a)** MR image when sensor is not in the room **b)** Image when the sensor is in zone I **c)** The subtraction a-b, the difference is 1.6%

(signal to noise ratio) definition of NEMA (National Electrical Manufacturers Association) is used [16].

Method of SNR Calculation

To have deeper information about the compatibility of force sensor, the SNR definition in National Electrical Manufacturers Association (NEMA) guidelines is used as follows [16]:

$$SD = \left[\frac{\sum_{i=1}^n \sum_{j=1}^{m_i} (v(i,j+1) - v(i,j))^2}{2 \sum_{i=1}^n (m_i - 1)} \right]^{\frac{1}{2}} \quad (2)$$

$$Noise = \frac{SD}{\sqrt{2}} \quad (3)$$

$$SNR = \frac{S}{Noise} \quad (4)$$

where:

n is the number of rows in the image

m_i is the number of columns in each row

$V(i,j)$ is the pixel value in the image of difference (a-b)

Figures 13, 14 and the calculated SNR values confirm that the sensor can be safely used in both MRI studies and surgical operations. For the first case (sensor in zone II), the SNR is 105.57 whereas SNR becomes 56.36 for the second case. Same type of calculations and tests have also been applied to ABS-plastic sensor but the SNR values were 49.7 and 86.9 respectively which are lower compared to the delrin sample. These experiments showed that the sensor does not affect the image significantly even when it is in the middle of the imaged area hence it can be safely used for even Zone I applications such as surgical operations.

VII. CONCLUSION

A sensing unit to be used in multi-axis force measurements is introduced in this paper. A genuine, compact and effective displacement amplification mechanism was designed for sensing applications and analyzed by finite element simulations. Amplification ratio of the device can be adjusted by changing several geometric parameters without compromising the compactness of the structure.

Two samples made of different materials, delrin and ABS-plastic, were tested and compared for their suitability for this application. Delrin sample is realized by water jet cutter whereas ABS-plastic sample is made by 3D prototyper. Delrin sensor, seen in Figure 15, is superior both in

mechanical performance and MRI compatibility compared to ABS-plastic unit.

Experiments showed that the sensor can decouple lateral and axial loads, which confirms that this idea can be used for multiple-axis applications. The sensitivity of the sensor in lateral direction is 1.66% of the sensitivity in axial direction. Initial linearity and hysteresis performance of the delrin sensor is promising. However, the overall stiffness of the delrin piece is higher than an acceptable value for a haptic device. In the future it is aimed to improve the force range and resolution of the device for haptic applications. To enhance the performance of the sensor, the hysteresis of 4.99% in the mechanical test data of delrin sample will also be analyzed. MRI tests confirmed that this sensor can be used for both MRI studies and surgical operations as the SNR values calculated for both applications are satisfactory. Besides improving the 1-axis sensing unit, it is aimed to expand this sensing idea to multi-axis. A combination of such sensing units can be arranged to get the desired number of freedom force sensors. Figure 16 illustrates two, triaxial sample configurations.



Fig. 15. The sensing unit made of delrin

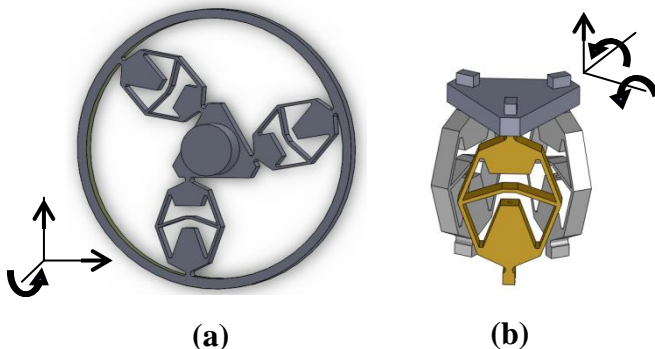


Fig. 16. Two different configurations of multi-axis sensing. The idea can be extended up to 6-axis sensing **a)** The proposed sensing units are in a coplanar configuration. This flat assembly is sensitive to planar forces and torsion. **b)** Another triaxial sensing configuration with three parallel sensing units for axial force and two types of moments is shown. A total of 6-axis sensing can be achieved if those suggested assemblies are integrated.

ACKNOWLEDGMENT

The authors would like to thank Dr. Robert J. Webster, III and Diana C. Cardona at Vanderbilt University for their valuable discussions.

REFERENCES

[1] R. Gassert, R. Moser, E. Burdet, H. Bleuler, "MRI/fMRI-Compatible Robotic System With Force Feedback for Interaction With Human Motion" in *IEEE Transactions on Mechatronics*, vol. 11, issue 2, pp. 216-224, April 2006.

[2] Z. Tsz Ho Tse, H. Elhawary, A. Zivanovic, M. Rea, M. Paley, G. Bydder, B. L. Davies, I. Young, M. U. Lamperth, "A 3-DOF MR-Compatible Device for Magic Angle Related In Vivo Experiments", in

IEEE Transactions on Mechatronics, vol. 13, issue 3, pp. 316-324, June 2008.

[3] C. R. Wagner, N. Stylopoulos, P. G. Jackson, R. D. Howe, "The Benefit of Force Feedback in Surgery: Examination of Blunt Dissection", *MIT Press Journals*, vol. 16, No. 3, pp. 252-262, June 2007.

[4] R. Gassert, D. Chapius, H. Bleuler, E. Burdet, "Sensors for Applications in Magnetic Resonance Environments", *IEEE Transactions on Mechatronics*, vol. 13, issue 3, pp. 335-344, June 2008.

[5] P. Puangmali, P. Dasgupta, L. D. Seneviratne, K. Althoefer, "Miniaturized triaxial optical fiber force sensor for MRI-Guided minimally invasive surgery", *2010 IEEE International Conference on Robotics and Automation (ICRA)*, pp. 2592-2597, May 2010.

[6] D. Chapuis, R. Gassert, L. Sache, E. Burdet, H. Bleuler, "Design of a simple MRI/fMRI compatible force/torque system", *IEEE International Conference on Intelligent Robots and Systems*, vol. 3, pp. 2593, Sept. 2004.

[7] A. Khanicheh, A. Muto, C. Triantafyllou, B. Weinberg, L. Astrakas, A. Tzika, C. Mavroidis, "MR Compatible ERF Driven Hand Rehabilitation Device", *IEEE 9th International Conference on Rehabilitation Robotics*, vol. 3, pp. 7-12, June 2005.

[8] U-Xuan Tan, B. Yang, R. Gullapalli, R. Desai, "Design and Development of a 3-Axis MRI-compatible Force Sensor" *IEEE International Conference on Robotics and Automation*, pp. 2586, May 2010.

[9] M. Tada, S. Sasaki, T. Ogasawara, "Development of an optical 2-axis force sensor usable in MRI environments", *Proceedings of IEEE, Sensors*, vol. 2, pp. 984, 2002.

[10] M. Tada and T. Kanade, "Design of an MR-compatible three-axis force sensor", *IEEE/RSJ Int. Conf. on Intelligent Robots and Systems*, pp. 3505-3510, 2005.

[11] N. Takahashi, M. Tada, J. Ueda, "An Optical 6-axis Force Sensor for Brain Function Analysis using fMRI", *Proceedings of IEEE, Sensors*, vol. 1, pp. 253, 2003.

[12] J. F. Schenk, "The role of magnetic susceptibility in magnetic resonance imaging: MRI magnetic compatibility of the first and second kind", *Medical Physics*, vol. 23, No. 6, June 1996.

[13] N. V. Tsekos, A. Khanicheh, E. Christoforou and C. Mavroidis, "Magnetic Resonance-Compatible Robotic and Mechatronics Systems for Image-Guided Interventions and Rehabilitation: A Review Study" in *Annual Review of Biomedical Engineering*, vol 9, pp. 351-387, April 2007.

[14] K. Chinzei, R. Kikinis, F. A. Jolesz, "MR Compatibility of Mechatronic Devices: Design Criteria" *Medical Image Computing and Computer-assisted Intervention-MICCAI'99 Lecture Notes in Computer Science*, vol. 1679/1999, pp. 1020-1030, 1999.

[15] M. Lazeroms, G. Villavicencio, W. Jongkind, G. Honderd, "Optical Fibre Force Sensor For Minimal-Invasive-Surgery Grasping Instruments", presented in *18th Annual International Conference of the IEEE Engineering in Medicine and Biology Society*, Amsterdam 1996.

[16] "Determination of Signal-to-Noise Ratio (SNR) in Diagnostic Magnetic Resonance Imaging", *NEMA Standards Publication MS 1-2001*, National Electrical Manufacturers Association